Colloids and Surfaces A 539 (2018) 69–79

Contents lists available at ScienceDirect

Colloids and Surfaces A

journal homepage: www.elsevier.com/locate/colsurfa

Synergetic effect of polyethylene glycol-grafted chitosan and bovine serum albumin on colloidal stability of polyelectrolyte nanocapsules

Tatsiana G. Shutava[a,*], Kanstantsin S. Livanovich[a], Vladimir V. Pankov[b]

[a] Institute of Chemistry of New Materials, National Academy of Sciences of Belarus, Minsk, Belarus
[b] Belarusian State University, Minsk, Belarus

GRAPHICAL ABSTRACT

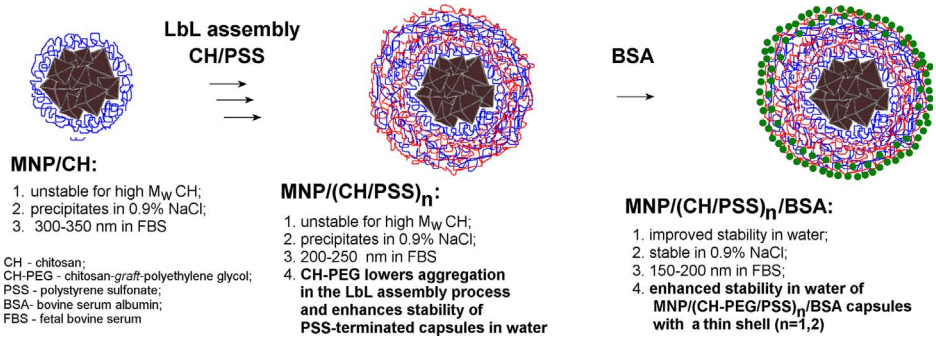

ARTICLE INFO

Keywords:
Layer-by-layer assembly
Nanocapsules
Polyelectrolyte
Polyethylene glycol
Chitosan
Copolymer
Polystyrene sulfonate
Magnetite
Bovine serum albumin
Colloid
Aggregative stability

ABSTRACT

Layer-by-layer (LbL) nanocapsules with a shell on the basis of chitosans (CH) of different molecular weights (CHx, hereafter x stands for M_w of the polysaccharide used), including those grafted with polyethylene glycol (CHx-PEG), and polystyrene sulfonate (PSS) were obtained on Mg-doped magnetite cores (MNP) and further coated with a layer of bovine serum albumin (BSA). The outermost BSA layer plays a key role in maintaining high aggregative stability of nanocapsules in 0.9% NaCl and preserving their low diameter in serum. The diameter of nanocapsules remains below 100 nm in the process of LbL assembly of low molecular weight CHx. The influence of polyethylene glycol-grafted CHx on the stability of LbL nanocapsules is contradictory. The co-introduction of two hydrophilic components, i.e. CHx-PEG and BSA, in the LbL shell supports high aggregative and sedimentation stability of the colloids, increases storage time of aqueous solutions of nanocapsules to the higher degree than each component on its own. The synergetic effect of copolymer and albumin on stability is especially noticeable for the nanocapsules containing one or two bilayers. By using PEG-grafted chitosans and BSA in one LbL shell, stable colloids of functional nanoparticles have been obtained in fewer adsorption cycles.

1. Introduction

Constructing nano-/microstructures with a desired size, shape, and function by utilizing biomolecules and mimicking biological systems has been recognized as being of great importance for many biomedical and technological applications [1–6]. Nanosized systems play a key role in the hierarchic organization of matter by bridging and overlapping the living and "non-living" levels. Self-assembly of biomolecules such as proteins and nucleic acids, lipids, polysaccharides, chlorophyll, etc. builds the foundation for the existence and effective functioning of

* Corresponding author.
E-mail addresses: tshutova@yahoo.com, shutova@ichnm.basnet.by (T.G. Shutava).

https://doi.org/10.1016/j.colsurfa.2017.12.008
Received 5 October 2017; Received in revised form 27 November 2017; Accepted 1 December 2017
Available online 05 December 2017
0927-7757/

living organisms [7,8]. Combination of nanotechnological principles for creation of submicron and nanoscale structures with chemical strategies for designing materials is an effective route to new assemblies with advanced properties. For example, programmable assemblies of DNA, proteins, and other molecules and stimuli-responsive functions can be achieved by means of appropriate molecular design [8,9]. Selective labeling of biomaterials allows for their effective sensing and altering interaction of cells with the assemblies for delivery of drugs to target sites in vivo [1,2].

Nanoparticles are in demand in many biomedical applications as contrast agents for magnetic resonance imaging, hypothermic substances for thermal ablation/hypothermia of tumor tissues, nanoparticulated forms of drugs for effective therapy, and fluorescent labels for diagnostic kits [1–4]. The benefits of nanoparticles include better safety versus standard therapies with patient survival rate being equivalent to standard treatments. The improved therapeutic efficacy of nanoparticulated drugs is based on enhanced permeability and retention effect, modified pharmacokinetics and tissue distribution as compared with free drug [6].

The colloidal stability and aggregation of nanotherapeutics have an impact on their biodistribution, pharmacokinetics, and systemic toxicity. However, their prediction remains substantially difficult due to complex influence of such factors as material, physicochemical properties of nanoparticles, presence of stabilizing agents and other components in solution, etc. A well-established approach designed to decrease aggregation of nanoparticles in complex biological media includes their electrostatic, steric, or electrosteric stabilization by a single polymer coating. Due to interaction with medium components the coating can become unstable or dissociate from the nanoparticles surface in high ionic strength liquids. It compromises stability of the colloids [2,10–12].

By forming a multilayered polymeric shell around core particles some properties of colloids can be significantly improved. Subsequently alternating layers of polymers with an overall thickness from one to few dozens of nanometers are organized on core surface by the layer-by-layer (LbL) assembly technique that integrates components of different nature (polyelectrolytes, proteins, etc.) in a single shell [13–18]. LbL assembly is based on electrostatic interaction of oppositely charged components that are adsorbed on the template surface in a predetermined order. LbL allows one to vary the composition of the formed coating by replacing one of the components by its modified counterpart and control thickness of the shell by increasing or decreasing the number of bilayers (n) in the assembly. The structure of polyelectrolytes and LbL shell architecture influence the dimensions of the obtained nanocapsules [14–16]. They can be reduced by utilizing low molecular weight polyelectrolytes [15–17] and modified LbL assembly methods, such as ultrasound-assisted LbL assembly, ultrafiltration etc. [17–23]. Recent progress in the field of LbL assembly includes biogenic capsules based on naturally occurring polymers (polysaccharides, proteins, DNA). The minimal toxicity and notable degradability of the biogenic capsules increases their potential application in the medicine, cosmetic, and food industry as compared with traditional polyelectrolyte capsules [24–26].

Nowadays nano- and microcapsules modified with polyethylene glycol (PEG), dextran, and polyvinyl alcohol are of great interest since the polymers change the character of surface interaction with proteins [17,27–30] and considerably lower aggregation of nanoparticles and microcapsules in salt and protein solutions [28,31]. Traditionally, PEG is introduced into LbL films by covalent grafting onto the target film surface [32] or by replacing polyelectrolyte in the terminal layer of the film by its PEG-modified counterpart [33,34]. The films having an outermost layer of PEG-grafted poly-L-lysine (PLL), poly-L-glutamic acid, polyethyleneimine, polyacrylic acid, or polyallylamine (PAH) are characterized by low adhesion of cells and proteins [34–38].

Block and graft copolymers of polyelectrolytes and hydrophilic nonionogenic oligomers, such as PEG, dextran, etc., were recently introduced in an LbL coating in the same way as unmodified polycations and polyanions, by alternating their adsorption with oppositely charged polymers [17,29]. While protruding into solution, PEG chains leave enough space for the countercharged polymer to diffuse toward free groups of outermost polyelectrolyte layer and form interpolyelectrolyte complex, thus allowing for film growth. For example, by alternate adsorption of components the films containing up to 10 bilayers of PAH and block-copolymer of polystyrene sulfonate (PSS) and poly(monomethoxypolyethylene glycol) acrylate have been obtained. The introduction of the copolymer increases the thickness of bilayer in the film with a factor of 1.5 as compared with PSS-based one [39]. The films containing up to 7 bilayers have been formed on the basis of block-copolymer of PLL and PEG alternated with heparin with a thickness comparable to that of the unmodified polyelectrolyte [17]. The coating partially reduced adsorption of bovine serum albumin (BSA). However, additional modification of the LbL film surface with covalently bound PEG was necessary to inhibit the adsorption of proteins from fetal bovine serum (FBS) [32].

A globular, water-soluble, unglycosylated serum protein albumin is frequently used for modification of surface properties of nanocapsules and diagnostic particles [40]. A layer of covalently or electrostatically attached albumin increases the intake of the modified nanovehicles by cells and enhances their accumulation in tumor tissue [41,42]. The specificity of albumin arising from its amino acid composition consists in its ability to form intermolecular complexes with both polycations and polyanions in solutions [43,44] and thin films [45,46]. On the other hand, it is known that the presence of BSA and other proteins in cell culture medium and serum significantly alters the aggregation behavior of nanoparticles. The formation of a so-called protein corona and bridging flocculation of nanoparticles by oppositely charged protein macromolecules can stabilize or collapse the colloidal system [10–12].

An incentive to undertake the research on colloidal stability on inorganic core-based nanocapsules was the choice of Mg-doped magnetite nanoparticles (MNP) as a perspective contrasting material for magnetic resonance imaging. For a number of $(Mg,Zn)_xFe_{3-x}O_4$ ($x \leq 0,3$) solid solutions, an increase of saturation magnetization was found as compared to non-substituted magnetite [47]. A study of the NMR relaxation of protons in aqueous solutions of MNP reveals that they show high r_1 and r_2 relaxation efficiency [48]. However, unmodified composite magnetite colloids have extremely low stability in aqueous solutions.

We report on the improved colloidal stability in biorelevant media of Mg-doped magnetite-based nanocapsules with a layer-by-layer shell on the basis of chitosans (CH) of different molecular weights (CHx, hereafter x stands for molecular weight of the polysaccharide used), including those grafted with PEG (CHx-PEG), and polystyrene sulfonate and further coated with a layer of bovine serum albumin (Fig. 1). The outermost BSA layer plays a key role in maintaining high aggregative stability of nanocapsules in 0.9% NaCl and, regardless of the shell structure, also contributes to the preservation of nanocapsules' diameter in FBS. The diameter of nanocapsules is below 100 nm in the process of LbL assembly of low molecular weight CHx, while the influence of PEG-grafted CHx on the stability of LbL nanocapsules is contradictory. The co-introduction of two hydrophilic components, i.e. CHx-PEG and BSA, in the LbL shell supports high aggregative and sedimentation stability of the colloids and increases storage time of aqueous solutions of nanocapsules to a higher degree than each component on its own.

2. Experimental

2.1. Materials

Chitosan of ca. 450 kDa (CH450, Sigma), monomethoxypolyethylene glycol (PEG, 5 kDa, Aldrich), sodium polystyrene sulfonate (PSS, 70 kDa, Sigma), poly(diallyldimethyl ammonium chloride) (PDDA, 100–200 kDa, Aldrich), bovine serum albumin (BSA, Sigma), κ-carrageenan (Fluka), phosphate buffered saline (PBS, Sigma),

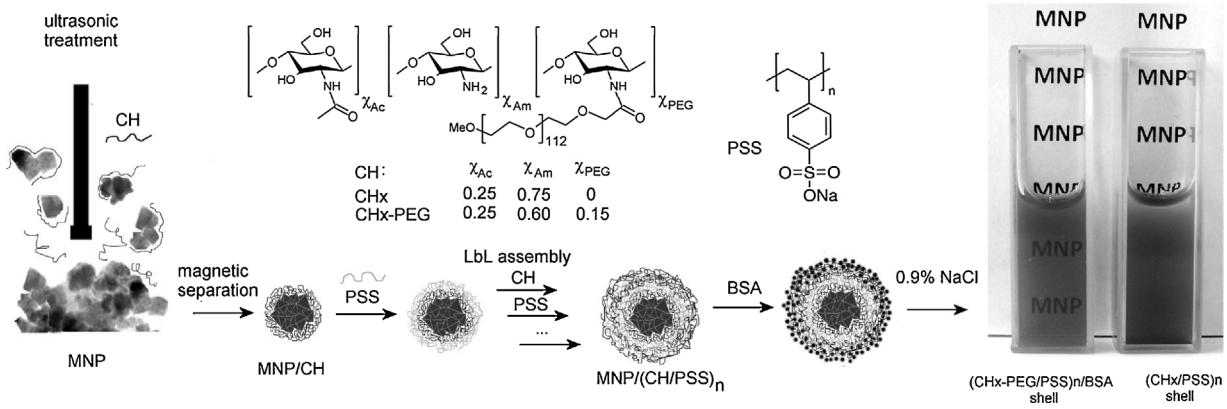

Fig. 1. Scheme of preparation of MNP/CH colloids and MNP/(CH/PSS)$_n$ nanocapsules.

Methylene Blue dye (MB, Sigma), 1-ethyl-3-(3-dimethylaminopropyl) carbodiimide (EDC, abcr GmbH) and N-hydroxysulfosuccinimide (sulfo-NHS, Thermo Scientific), fetal bovine serum (FBS, HyClone, GEHealthcare, South America origin) were used without further purification.

2.2. Preparation of chitosans of different molecular weight

Depolymerized chitosans of 18 kDa (CH18) and 60 kDa (CH60) were obtained by treating a 0.75% CH450 solution in 1% acetic acid (200 mL) with hydrogen peroxide taken in excess for a given period of time at 50 °C according to [29]. The chitosans were precipitated from the reaction mixtures by aqueous ammonium hydroxide and acetone, separated by centrifugation, washed twice with acetone dried at ambient temperature for 12 h and then lyophilized. The molecular masses of original and depolymerized chitosans were determined by measuring solution viscosity of their 0.0125–0.5% solutions in 1% acetic acid through a capillary viscometer and calculating according to the Mark-Kuhn-Houwink equation ($K = 1.38 \cdot 10^{-4}$ cm^3/g; $\alpha = 1.02$) [49].

The FTIR spectra of polymers were recorded using a *Tensor 27 Bruker* instrument in KBr tablets. The assignment of absorbance bands in the IR spectrum of chitosan was made according to [50,51]. The degree of acetylation (χ_{Ac}) of chitosan was calculated as:

$$\chi_{Ac} = A_{1655}/A_{3450} \cdot 1/1.3, \quad (1)$$

where A_{1655} and A_{3450} are the intensities of 1655 and 3450 cm^{-1} bands in the IR spectrum of the polymer [50].

2.3. Preparation of CHx-PEG

Polyethylene glycol with terminal carboxylic group (cPEG) was obtained as described elsewhere [52]. PEG of 5 kDa (5 g) was dissolved in distilled water (50 mL). 0.16 g of $KMnO_4$ dissolved in 20 mL water was added to the solution, followed by 5 mL of a 40 mg/mL $CaCl_2$ solution to accelerate PEG hydroxyl group oxidation [53]. The reaction mixture was kept at 40 °C for one hour. The formed dark-brown precipitate was discharged. The filtrate was acidified to pH < 3 with a few drops of 5 N HCl and extracted twice with 50 mL of dichloromethane. The organic phases were combined and solvent was evaporated under reduced pressure. The presence of carboxylic groups in cPEG was confirmed by FTIR spectroscopy; their concentration was evaluated through colored iron – hydroxamic acid complex formation using acetic acid as a standard for quantification [54]. The retention of average molecular mass of cPEG was confirmed by viscometry using polyethylene glycols of 1.5 and 5.0 kDa as standards for evaluation of the coefficients in the Mark–Kuhn–Houwink equation.

CHx-PEG copolymers were obtained in phosphate buffered saline (pH 7.4) using EDC and sulfo-NHS as crosslinking agents [55]. CHx was dissolved in 1% acetic acid. A 25 mg/mL cPEG solution was added to an equal volume of 5 mg/mL chitosan to obtain the required molar ratio of cPEG and glucosamine units in the reaction mixture (8 mL), then sequentially EDC and sulfo-NHS in PBS buffer (0.2 mL, 0.2 M each) were admixed. The mixture was vigorously shaken and left for 3 h at room temperature. The reaction mixture was dialyzed against water for 48 h using a MWCO 10 kDa Snake Skin Thermo Scientific tubing and lyophilized.

The attachment of PEG chains to CHx was confirmed by FTIR. The amounts of free $-NH_2$ groups in CHx and CHx-PEG were determined using the MB-κ-carrageenan complex [29,56]. The stock-solution was prepared by mixing 49.5 mL of an MB solution in 1% acetic acid (the absorbance of this solution at 665 nm (A_{665}) was adjusted to 1.00 ± 0.05) and 3.5 mL of a 1 mg/mL κ-carrageenan solution. In the spectrum of the mixture, the band at 665 nm that corresponds to free MB molecules decreased and absorbance at 566 nm (A_{566}) attributed to the dye complexed with sulfo groups of κ-carrageenan appeared. The titer (T) of the stock-solution estimated on PAH is 0.107 mM. To perform the analysis, 0.01 ÷ 0.50 mL of a copolymer solution was added to 2 mL of the stock-solution and the total volume of the mixture was adjusted to 3 mL with 1% acetic acid. The solutions were vigorously mixed and their absorbance spectra were recorded in the range of 450–750 nm. The dependence of A_{566}/A_{665} on the concentration of corresponding polymers was plotted. The concentrations $C_{CHx\text{-}PEG}$ and C_{CHx} at which the copolymer CHx-PEG under investigation and the unmodified chitosan CHx completely displace MB from its complex with κ-carrageenan were obtained from the graphs (Fig. SI 1).

The share of PEG-modified amine groups in copolymer (χ) was calculated as:

$$\chi = N/(T + N); \; N = (C_{CHx\text{-}PEG} - C_{CHx})/(M_w^{PEG} + C_{CHx}/T). \quad (2)$$

The share of *N*-glucosamine units in copolymer substituted with PEG was calculated as

$$\chi_{PEG} = \chi \cdot (1\text{-}\chi_{Ac}). \quad (3)$$

2.4. Preparation of MNP/CH colloids

Magnesium-doped magnetite $Mg_{0,1}Fe_{2,9}O_4$ was synthetized by co-precipitation of metal salts with sodium carbonate in a basic solution. Magnetite colloids with the dispersed phase coated with a polycation layer (MNP/CH, CH═CHx or CHx-PEG) were obtained by ultrasonication [48]. A suspension (~20 mL) containing 0.15 mg/mL magnetite and 3 mg CH per 1 mg of dispersed phase was treated for 2 min in a *Sapphire* ultrasonic bath (35 kHz working frequency), then 4–5 times for 45 s each using an *UZG-13-0,1/22* immersible ultrasonic disperser (22 kHz working frequency), followed by a 2 min treatment in the bath. To prevent overheating the suspension was cooled down on an ice-bath.

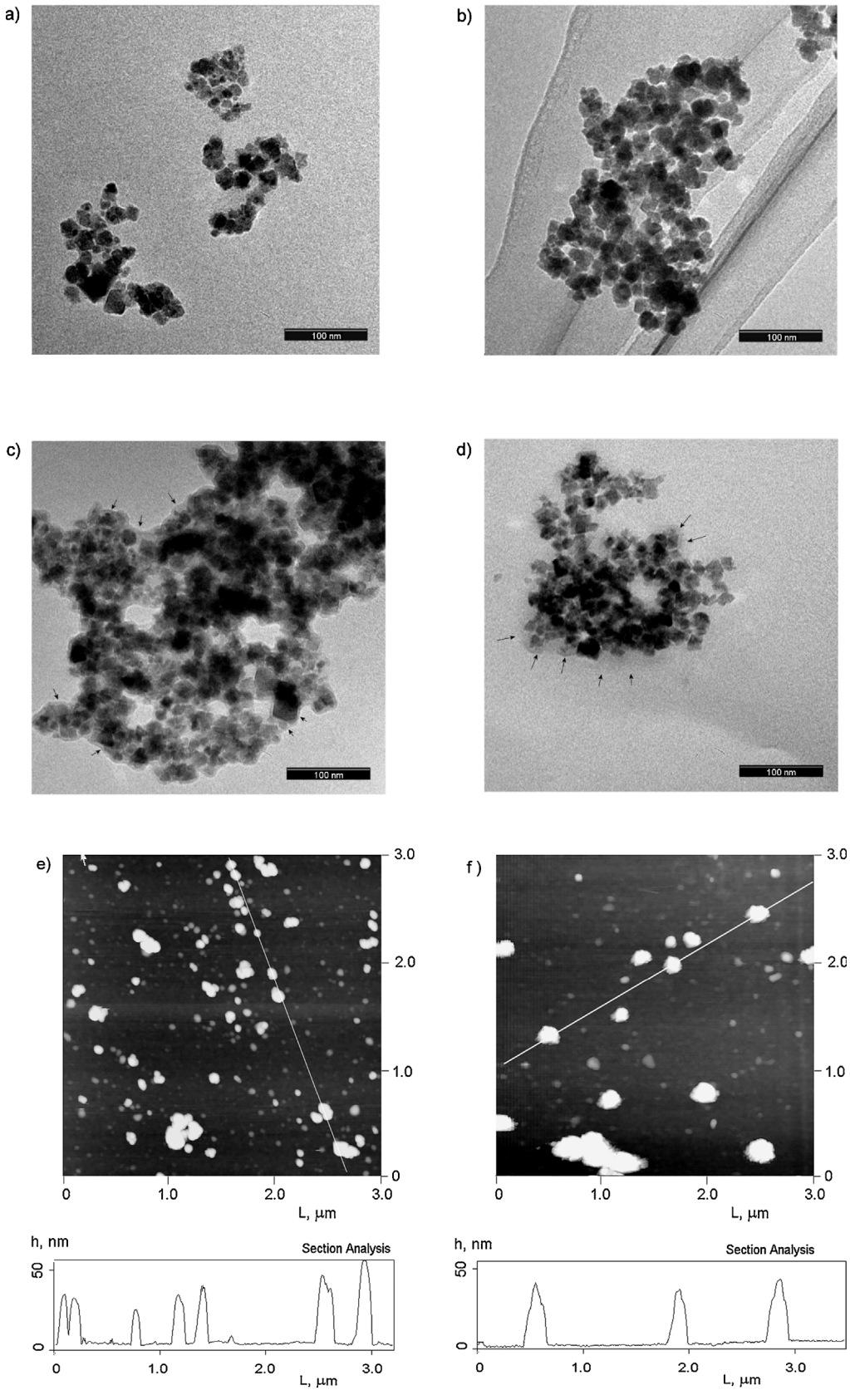

Fig. 2. a–d) TEM images of MNP/PDDA, (c, DLS: d = 55 ± 4 nm, PDI = 0.16), MNP/CH60-dextran 6 kDa, (d, DLS: d = 150 ± 10 nm, PDI = 0.14, $\chi_{dextran}$ = 0.15), MNP/(CH60-PEG/PSS)$_4$ (e), and MNP/(CH60-PEG/PSS)$_4$/BSA (f). The LbL shell boarder is indicated by arrows. e–f) AFM images of MNP/CH18 nanoparticles (a) and MNP/(CH60-PEG/PSS)$_2$ nanocapsules (b). The height profile across the indicated line is shown below each image.

Nanoparticles coated with a CH layer were separated over a permanent magnet and dispersed in distilled water as a 0.5 mg/mL solution as recalculated to magnetite. The concentration of magnetite in the dispersions was determined using *o*-phenanthroline [57].

2.5. Preparation of MNP/(CH/PSS)$_n$ nanocapsules

A shell consisting of 1–4 bilayers of CH and PSS was formed around MNPs using the layer-by-layer assembly technique [17,18,32].

Typically, 50 μL of a 5 mg/mL PSS solution was added to 5 mL of a MNP/CH colloid. The mixture was ultrasonicated in the bath for 30 s to avoid particle aggregation. The obtained nanocapsules were separated using a permanent magnet and redispersed in water without intermediate washings. The next CH layer on the surface of the nanocapsules was formed in a similar way. A CH solution was added to the dispersion of nanocapsules to achieve a 0.5 mg/mL concentration. The alternated adsorption of polyelectrolytes continued until a shell with a given number of bilayers n was obtained around the magnetic cores. The integer values of n correspond to $(CH/PSS)_n$ nanocapsules the outermost shell layer of which is comprised of PSS. The half-integer values of n relate to CH-terminated shells. BSA was added to the nanocapsules at a final concentration of 1.0 mg/mL.

The colloidal stability of nanocapsules was tested in H_2O, 0.9% NaCl solution (at 25 °C), and FBS (at 37 °C). The value of ζ-potential of the nanocapsules was measured 10 min after admixing 50 μL of nanocapsules to 1 mL of the investigated medium, the diameter – at predetermined time intervals. The concentration of nanocapsules in the mixture was ~0.1 mM as recalculated to Fe or ~25 mg/L as recalculated to Mg-doped magnetite. The turbidity of FBS during its incubation with the nanocapsules was followed at 600 nm on a *CM2203 Solar* spectrofluorometer.

The hydrodynamic diameter, polydispersity index (PDI) and ζ-potential of nanoparticles and nanocapsules were measured using a *ZetaSizer NanoZS Malvern* analyzer. The size distribution of nanocapsules was obtained using the standard instrument software. The diameter *d* corresponds to the size of the most abundant number fraction of particles in a sample. The size of nanocapsules in FBS was characterized by the position Z of corresponding maximum on the diagram of light scattering by intensity. The values of 1.670 cP and 1.350 were used for viscosity and refractive index of FBS respectively. All measurements were done for three independent preparations of nanocapsules with a given shell structure. Each of them taken separately was measured three times using averaging for 7 runs of 5 s each. The average value for the three preparations is shown on diagrams and graphs; error bars represent standard deviation.

Size and morphology of the particles were examined by transmission electron microscopy (TEM) using a LEO 906E microscope. The atomic force microscopy (AFM) images of MNP/CH and MNP/$(CH/PSS)_n$ were obtained on a *MultiMode Nanoscope III Veeco* scanning probe microscope using silicon nitride probes in a continuous height-friction dual mode. A drop (20 μL) of the sample under investigation was placed on a wet silicon wafer precoated with a $(PDDA/PSS)_3$ LbL film for 10 min, then the wafer was rinsed with water and dried in upward position for 24 h before scanning. The images were processed using the Nanoscope v531 software.

3. Results and discussion

For the modification of MNP, chitosans of different molecular weight have been obtained. All chosen CH including synthetized copolymers (Fig. 1) had similar degree of acetylation of glucosamine units, ca. 0.25 ± 0.02. The part of polymer backbone units conjugated with PEG χ_{PEG} in CHx-PEG is ca. 0.15 ± 0.01. It corresponds to the grafting degree (g) equal to 5. There is one PEG chain in copolymer grafted per every five deacetylated amino groups in parent chitosan. Thus, the part of unsubstituted glucosamine units χ_{Am} in the CHx-PEG copolymers reaches 0.60. These amine groups are available for intercomplexation with sulfo groups of PSS.

3.1. Morphology of MNP/CH colloids and MNP/$(CH/PSS)_n$ nanocapsules

The grain size in the Mg-doped magnetite prepared by carbonate coprecipitation is about 20 nm (Fig. 2a–d). However, its aqueous suspensions are unstable. The hydrodynamic diameter of MNP without stabilizing agent exceeds 2.0 μm [48]. During the sonication of a MNP suspension in a solution of positively charged polyelectrolyte, such as PDDA or CH, macromolecules adsorb on the newly formed core surface preventing the coalescence of the formed nanoparticles. The cores in both MNP/CH colloids and MNP/$(CH/PSS)_n$ nanocapsules appear to acquire irregular shape and consist of several grains of Mg-doped magnetite (Figs. 2a,b, SI 2).

The LbL shell forms on the surface of the grain aggregates exposed to the media including open mesopores and covers protrusions and recesses as indicated by arrows (Fig. 2c,d). The thickness of the LbL shell consisting of four CH60-PEG/PSS bilayers calculated on the basis of the TEM images is about 8 nm. After the adsorption of BSA it increases and reaches 14–18 nm. The values are in good agreement with the bilayer thickness of copolymer-based LbL films obtained by the quartz crystal microbalance technique [29].

Due to irregular shape of the MNP cores, both MNP/CH colloids and MNP/$(CH/PSS)_n$ capsules possess uneven surface as it appears in the corresponding AFM images (Fig. 2e,f). The majority of MNP/CH particles have vertical dimensions within 30–60 nm. It agrees well with the diameter of most abundant number fraction of the particles in the colloids as determined by dynamic light scattering (DLS). In all MNP/CH colloids, there is a minor fraction of particles smaller than 30 nm in size. The aggregates with a diameter below 10 nm in the AFM images are associated with soft PDDA/PSS interpolyelectrolyte complexes formed on the LbL-precoated surface (Figs. SI 3, SI 4). The height of MNP/$(CH/PSS)_n$ nanocapsules calculated from their profile is in the range of 40–70 nm (Fig. 2b). The lateral dimensions of the dried capsules are within 150–250 nm. Larger particles with dimensions above 250 nm are a result of nanocapsules aggregation upon drying.

3.2. MNP/CH colloids

The MNP/CH colloids with a diameter of the disperse phase lower than 100 nm were prepared by sonicating MNP suspension in a solution of any of three unPEGylated chitosans CHx or copolymer CH18-PEG (Fig. 3a–f, for n = 0.5, t = 0). The diameter of particles obtained in CH450-PEG and CH60-PEG is larger than 220 nm presumably due to high molecular weight of the copolymers (~ca. 10^6 Da and 10^5 Da respectively). The PDI values for all obtained MNP/CH colloids are below 0.3 indicating that they have a narrow, close to monodisperse, particle size distribution (Fig. SI 5).

A slightly negative ζ-potential of unmodified MNP changes to a high (for CHx) or moderate (for CHx-PEG) positive value for MNP/CH colloids (Fig. 4). Despite a rather high ζ-potential of MNP/CH450, which is equal to +22 ± 2 mV, the colloid rapidly loses its aggregative stability. After the particles being stored for 24 h in water, their size exceeds 1 μm (Fig. 3a, n = 0.5). A decrease of MNP/CH450 particles diameter observed on the fifth day after their preparation is associated with irreversible sedimentation of large aggregates. The colloids stabilized by depolymerized chitosans CH60 and CH18 have ζ-potential value comparable to that of MNP/CH450. However, there is no significant increase of their diameter after two weeks of storage. The difference can apparently be explained by partial desorption of long CH450 macromolecules from the surface of MNP. The polymer later adsorbs and bridges neighboring nanoparticles. The process results in a rapidly increasing number of aggregates. Due to lower values of the ζ-potential (Fig. 4c) MNP/CHx-PEG colloids gradually lose aggregative stability (Fig. 3d–f, n = 0.5). An increase of hydrodynamic diameter of the particles is accompanied by rising PDI value (Fig. SI 5, c).

3.3. Influence of BSA on MNP/CH stability

By dispersing magnetite directly in a BSA solution the particles with a mean diameter of 350–380 nm having a wide size distribution have been prepared. The obtained dispersions of MNP/BSA are unstable and magnetic phase in them rapidly precipitates [47].

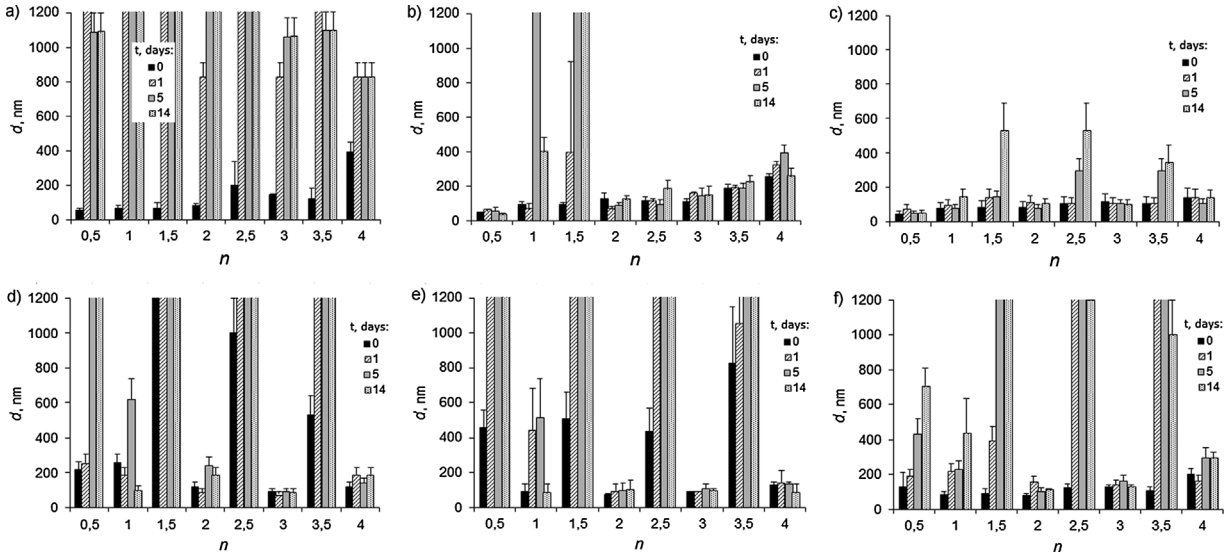

Fig. 3. Diameter of MNP/$(CH/PSS)_n$ nanocapsules at different times. CH: a – CH450; b – CH60; c – CH18, d – CH450-PEG, e – CH60-PEG, f – CH18-PEG. H_2O, 25 ± 3 °C. The height of the value axis is limited because of the incorrectness of determination of *d* for rapidly precipitating particles aggregates.

The addition of BSA into a MNP/CH colloid produces particles with a diameter larger than 400 nm (Fig. 5a–f, n = 0.5, t = 0) with the exception of those of low molecular weight chitosan CH18. For the latter, the diameter increased from 44 ± 9 nm to 93 ± 19 nm. According to DLS, the fraction of particles with a diameter of 5–7 nm corresponding to BSA macromolecules is absent in all prepared MNP/CH/BSA colloids. The observed changes of the ζ-potential from a highly positive for MNP/CH to a weakly negative value for MNP/CH/BSA are consistent with the adsorption of thick albumin corona on the particle surface (Fig. 4). Isoelectric point of bovine serum albumin is about 4.2 [40] and at the near-neutral pH the protein is negatively charged. The ζ- potential of BSA in water measured under experimental conditions is −7.8 ± 0.7 mV.

With increasing storage time, the diameter of MNP/CH450 and MNP/CH450-PEG particles on which BSA is adsorbed decreases to 320–400 nm, while for MNP/CH60-PEG it reaches ~100 nm. In contrast to this, for other chitosans and copolymers, increasing aggregation of the particles was observed upon storage (Figs. 5, SI 5, c,d). Negatively charged BSA macromolecules in protein corona apparently compete with low charged surface of MNP for complexation with CH

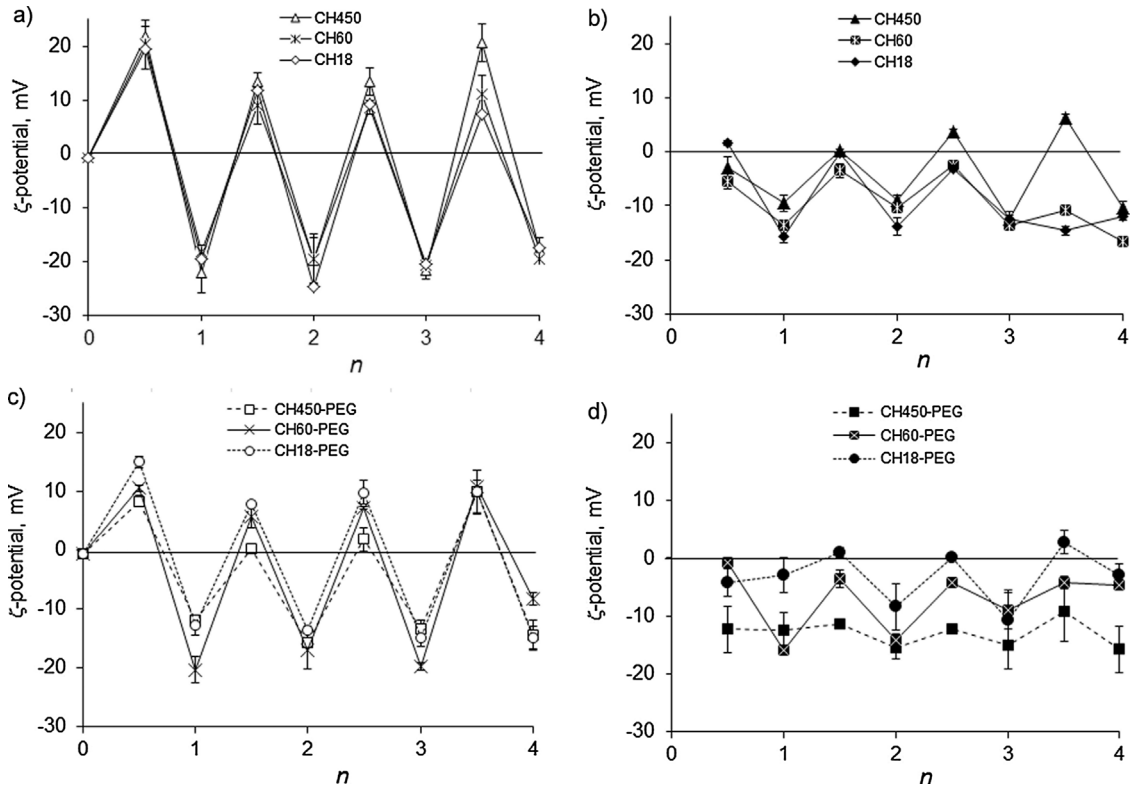

Fig. 4. ζ-potential of nanocapsules with a $(CH/PSS)_n$ (a, c) and $(CH/PSS)_n$/BSA (b, d) shell.

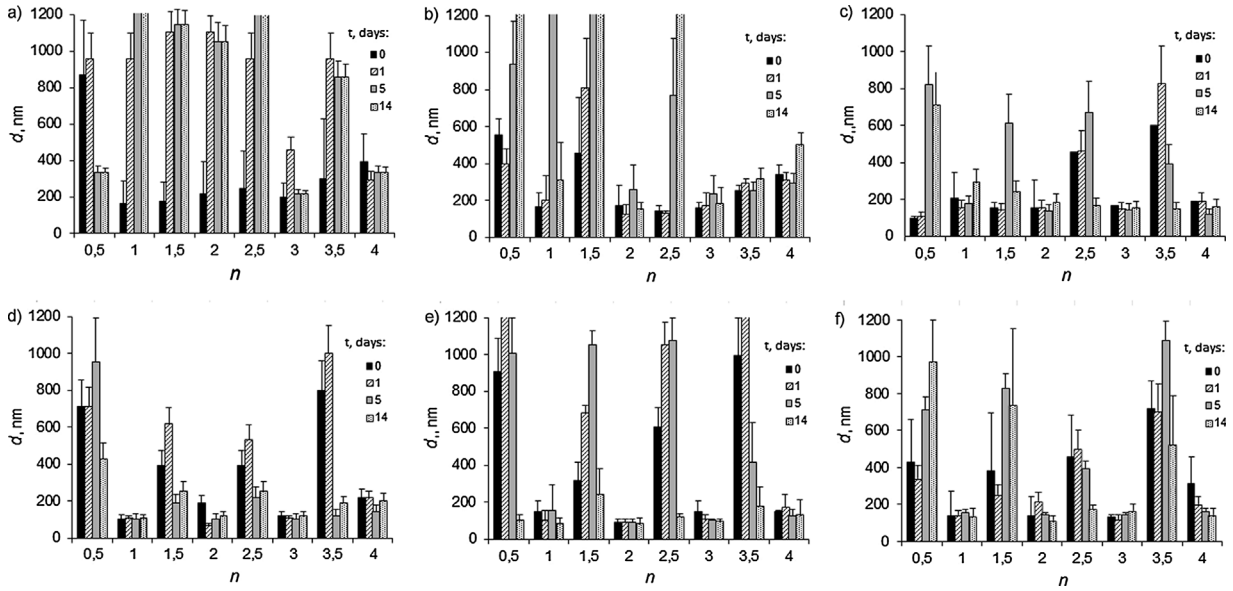

Fig. 5. Diameter of MNP/(CH/PSS)$_n$/BSA nanocapsules at different times. CH: a – CH450; b – CH60; c – CH18; d – CH450-PEG, e – CH60-PEG, f – CH18-PEG. H_2O, 25 ± 3 °C.

and disturb adsorbed layers of low molecular weight chitosans to a higher degree [43].

3.4. MNP/(CH/PSS)$_n$ nanocapsules

The (CH/PSS)$_n$ shells were formed around Mg-doped magnetite nanocores by LbL assembly of the polyelectrolytes (Fig. 1). The alternating ζ-potential of nanocapsules in the process of sequential adsorption of positively charged CH and negatively charged PSS confirms the formation of multilayered shell (Fig. 4).

An increase of the diameter of MNP/(CH/PSS)$_n$ nanocapsules with increasing number of adsorbed layers is pronounced for chitosan CH450 and sufficient for CH60. Such changes are associated with a small number of aggregates formed on each stage of adsorption of the unmodified polysaccharides (Fig. 3a, b, t = 0). For all the nanocapsules, a gain in the hydrodynamic diameter is accompanied by an increase of polydispersity. The typical changes of polydispersity indexes are uillustrated in Fig. SI 5 on the example of CH60 and CH60-PEG–-based capsules. The diameter of MNP/(CH18/PSS)$_n$ and MNP/(CH18-PEG/PSS)$_n$ nanocapsules also increases with increasing n, but for a four-bilayer shell it remains lower than 150 nm (Fig. 3c, f, t = 0). Despite comparable PEG grafting of all CHx-PEG copolymers, the longer glucosamine chain promotes formation of aggregates in the case of nanocapsules with a CH450-PEG and CH60-PEG-terminated shell (Fig. 3d, e, t = 0). After adsorption of the next PSS layer the low diameter of the nanocapsules is restored. It is worth noting that if one takes into account only PSS-terminated shells the diameter of all (CHx-PEG/PSS)$_n$ nanocapsules increases slightly with increasing n. Moreover, by using CHx-PEG in the PSS-terminated shell instead of unmodified chitosan the nanocapsules with a narrower size distributions are obtained (Fig. SI 6). The fraction of nanocapsules with a diameter above 200 nm is practically absent in the samples.

Regardless of the shell structure, the MNP/(CH450/PSS)$_n$ nanocapsules based on chitosan with long glucosamine chain aggregate within 24 h after preparation with a significant fraction of sediment (Fig. 3a). In the case of CH60, the diameter of nanocapsules containing 2 or more bilayers remains low during the whole observation period (Fig. 3b), while for CH18, the diameter of CH18-terminated capsules slightly increases with time (Fig. 3c).

The size of any nanocapsule with a CHx-PEG upper layer in water rapidly reaches values exceeding 1.2 μm (Fig. 3d–f). At the same time, PSS-terminated MNP/(CHx-PEG/PSS)$_n$ nanocapsules with an integer n are more stable, and for n = 2,3, or 4 their diameter does not practically change within all observation period. Regardless of molecular weight of glucosamine chain CHx-PEG nanocapsules with a one bilayer shell retain low diameter only for limited time, and then it increases above 600 nm.

3.5. Influence of BSA on MNP/(CH/PSS)$_n$ nanocapsules stability

If one compares the graphs in Figs. 3 and 5, one can see the effect of BSA on the initial diameter and the aggregative stability of nanocapsules. The adsorption of BSA on the surface of CHx-based nanocapsules results in an increase of the diameter of both CHx and PSS terminated ones by 50–200 nm (Fig. 5a–c, t = 0). For CHx-PEG–based nanocapsules, an alternation of the lower and higher diameter of nanocapsules as a function of BSA-preceding polyelectrolyte has been found (Fig. 5d–f, t = 0). The polypeptide chain of BSA allows the protein to form complexes with both polycation and polyanion on the surface of nanoparticles [44–46]. The presence of hydrophobic domains in the albumin and the ability to form intermolecular hydrogen bonds by a number of amino acids [58,59] seem to facilitate the association of BSA with PEG on the surface of copolymer-terminated nanocapsules. Their size sufficiently increases.

If albumin is adsorbed on a CHx layer the aggregation of the nanocapsules intensifies with time as compared with the nanocapsules without BSA (Fig. 5a–c). The effect of BSA on the stability of PSS-terminated capsules is less distinct.

Unlike the CHx-based nanocapsules, the adsorption of BSA on the surface of nanocapsules on the basis of copolymer improves the stability of both CHx-PEG and PSS-terminated capsules (Fig. 5d–f). Furthermore, the aggregation of nanocapsules with the outermost layer of CHx-PEG in the presence of BSA becomes reversible. Initially increasing diameter of the nanocapsules decreases if the storage time increases and no precipitate forms during all observation period. The effect of copolymer and albumin on the storage stability of MNP/(CHx-PEG/PSS)$_n$/BSA nanocapsules is especially evident for the shells with a small number of bilayers. BSA considerably increases stability of the nanocapsules the shell of which contains one bilayer of CH18-PEG or CH60-PEG. For high molecular weight copolymer CH450-PEG, the synergism of BSA and copolymer can be traced to the second bilayer.

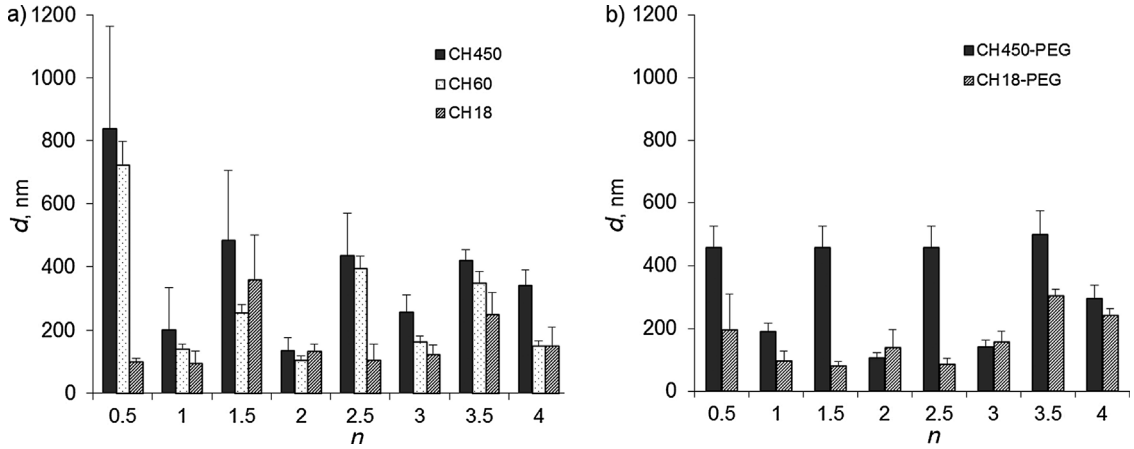

Fig. 6. Diameter of nanocapsules with a $(CH/PSS)_n$/BSA shell in 0.9% NaCl. a) CHx; b) CHx-PEG.

3.6. Nanocapsules in 0.9% NaCl

All MNP/CH colloids and MNP/$(CH/PSS)_n$ nanocapsules aggregate fast in 0.9% NaCl, with no respect to the polyelectrolyte shell structure or polycation used. Their effective diameter reaches 0.5-2.0 μm 10 min after mixing followed by solid phase precipitation. High values of polydispersity index (PDI > 0.4) and standard deviation (up to 0.4 μm) of diameter for the nanocapsules confirm increased sample aggregation.

At the same time, the diameter of MNP/$(CH/PSS)_n$/BSA nanocapsules, in which BSA is adsorbed on a PSS layer, in 0.9% NaCl does not change relatively to that in water (Fig. 6). If a CH layer comes before adsorption of BSA, the diameter of the nanocapsules in isotonic salt solution increases, but BSA prevents their irreversible sedimentation. The highest stabilizing effect of albumin was found in the case of CH18 and CH18-PEG-based nanocapsules. The alternation of the diameter of PSS and CH-terminated shells for them was minimal.

3.7. Nanocapsules in FBS

The light scattering maximums of fetal bovine serum are located at 5.3 ± 2.2 nm for the albumin and 35.3 ± 21.5 nm for the globulins/lipoproteins fraction respectively. The addition of distilled water in the amount of 50 μL/mL does not change the positions of the peaks. A prominent maximum Z appears in the region of 150–320 nm if MNP/CH nanoparticles or MNP/$(CH/PSS)_n$ nanocapsules are added. Regardless of the length of glucosamine chain and the presence of PEG grafting on CH, the value of Z for the CH-terminated nanocapsules in FBS is 50–75 nm larger than that of nanocapsules with a PSS layer on the surface (Fig. 7a). Apparently, this is due to the peculiarities of adsorption of various FBS protein fractions (albumins and immunoglobulins) on positively and negatively charged surfaces [21,31,32]. At the same time, for MNP/$(CH/PSS)_n$/BSA nanocapsules the effect of the layer preceding albumin on Z in FBS is negligible.

MNP/CH colloids incubated in FBS at 37 °C retain a 300–350 nm size for 6–8 h. The changes of the diameter of MNP/$(CH/PSS)_n$ nanocapsules depend on the polyelectrolyte adsorbed on their outermost surface. The size of PSS-terminated ones (an integer *n*) in FBS does not practically change with time; even one CH/PSS bilayer is sufficient to stabilize nanocapsules. For CH-terminated nanocapsules, Z decreases from 270 to 340 nm to 150–200 nm after incubation for 2–4 h (Fig. 7b). The observed regularities can apparently be explained by the interaction of FBS proteins, mainly albumin, with the polyelectrolyte shell. Slowly diffusing into the inner shell layers towards the core proteins stabilize it. The peptization of the particles occurs with time. Regardless of the BSA-preceding layer the diameter of MNP/$(CH/PSS)_n$/BSA nanocapsules does not change in FBS for 6–8 h. Moreover, the changes of the turbidity of FBS to which nanocapsules are added are negligible. Therefore, large proteins/nanocapsules aggregates are absent.

In respect to the diameter of LbL nanocapsules in serum, there is no advantage of copolymer-based shell over those of chitosan. Nevertheless, we presume that LbL shells based on copolymers are prospective for controlling the interaction of nanocapsules with the body's immune system and distribution in tissues. For instance, an inhibition of the FBS protein adsorption by (CHx-PEG/dextran sulfate)$_n$ films has been shown on planar surface [29]. Dextran-coated and polyvinyl alcohol-coated SPIONs demonstrate selective adsorption of serum proteins [60].

3.8. Mechanism of MNP/$(CH/PSS)_n$ nanocapsules stabilization

Due to multicomponent shell structure the mechanism of stabilization of the LbL nanocapsules has a complex character. For unmodified chitosans CHx, the stability of MNP-based nanocapsules can apparently be fully described in terms of electrostatic repulsion between charged surfaces (Fig. 8). Bridging neighboring capsules by long polyelectrolyte chains explains low stability of CH450-based capsules. The influence of steric stabilizer PEG as a result of CHx-PEG introduction into the LbL shell manifests itself only in the combination with strong negative charge of outermost PSS layer (electrosteric stabilization). The effect is revealed in small nanoparticles diameter maintained in the LbL assembly process and long term colloidal stability of the nanocapsules. Despite of CHx-PEG attached as an outermost layer, copolymer-terminated nanocapsules are partially aggregated due to relatively low surface charge brought by PEG-substituted glucosamine chains to the surface.

The hydration of upper layers of a LbL shell can be as high as 40–50% v/v and decreases in the vicinity of the core to 20–26% [61,62]. In addition, PEG binds at least one water molecule per every PEG monomer unit due to hydrogen bonding [63]. However, no data on the MNP nanocapsules stability can be interpreted so far as being affected to a passable degree by high hydration of LbL shell material.

On the other hand, the anomalous colloidal stability of BSA-modified nanocapsules that have a rather low ζ–potential can be explained in terms of hydration forces, especially at high ionic strength in 0.9% NaCl. The water binding capacity of albumin is exceptionally high. Albumin is capable of holding up to 18 mL water per gram within the vascular space [64]. The hydration water layer around BSA extends as far as 1.5–2.5 nm from the protein and includes up to 20,000 water molecules per one BSA macromolecule [65–67]. Sodium and other small ions tend to accumulate in the vicinity of protein core and increase albumin's capacity of binding water in salt solutions (the Gibbs-Donnan effect) [68].

A significant difference in stability of CHx-terminated (Fig. 3d–e) and CHx-PEG-terminated (Fig. 5d–e) nanocapsules is observed after

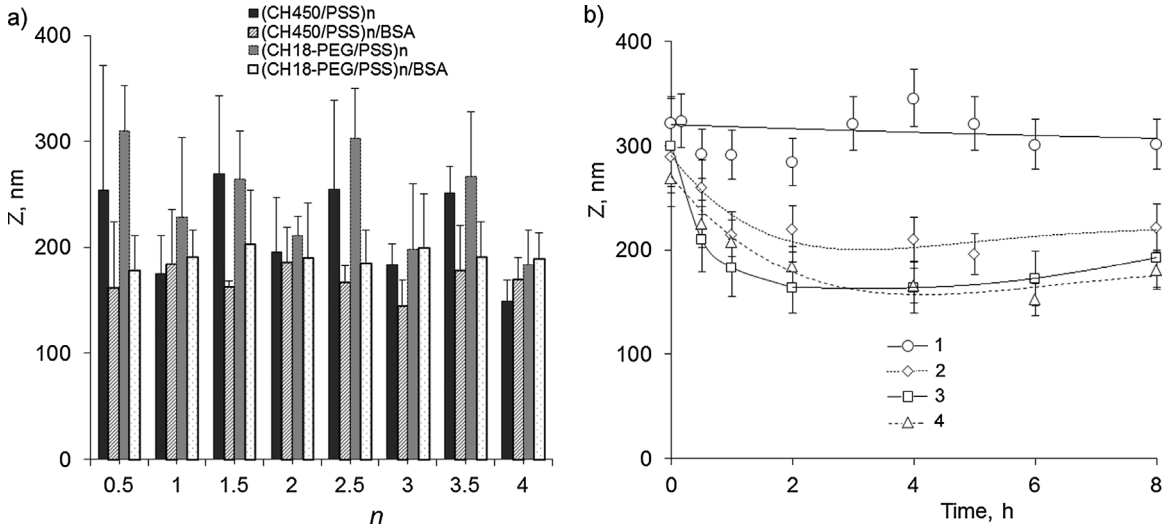

Fig. 7. Diameter Z of MNP/$(CH/PSS)_n$ nanocapsules in FBS: a) with different shell structure incubated for 10 min, b) with a $(CH450/PSS)_n$ shell, n: 1–0.5; 2–1.5; 3–2.5; 4–3.5. Temperature 37 °C.

their modification with a BSA corona. For the shells with relatively *high PEG surface density*, we assume a brush conformation of PEG side chains. The distance between PEG grafts and the length of PEG brushes depend on the adsorbed amount of copolymer. The latter increases with increasing the number of bilayers in a LbL shell. The Flory radius of 5 kDa PEG molecules is 5.96 nm [69], while the calculated contour length can be as high as 40 nm [55]. The thickness of a BSA corona on the surface of nanocapsules is 6–10 nm as calculated from the TEM data. The value of a BSA layer thickness estimated with the assumption of complete adsorption of the protein on 100–200 nm shells is from 5 to 16 nm. Thereby the values are of the same order of magnitude. After adsorption of BSA the PEG chains are apparently surrounded by a thick protein layer. The combination of highly hydrated BSA layer and steric repulsion of PEG tails results in the stabilization of the nanocapsules.

After adsorption of one CHx-PEG/PSS bilayer PEG chains are loosely distributed over the MNP surface. At *low surface density*, PEG chains tend to be in a mushroom conformation which does not support high adsorption resistance [69]. BSA fills the gaps between the scattered PEG chains forcing them to take an extended conformation. The effect of hydration water layer of BSA is combined with steric hindrance due to protruding PEG tails. Combined the copolymer and BSA stabilize nanoparticles to a higher degree than each component on its own.

The improvement of the diameter of BSA-modified capsules with time can be explained by the influence of different factors. Albumin

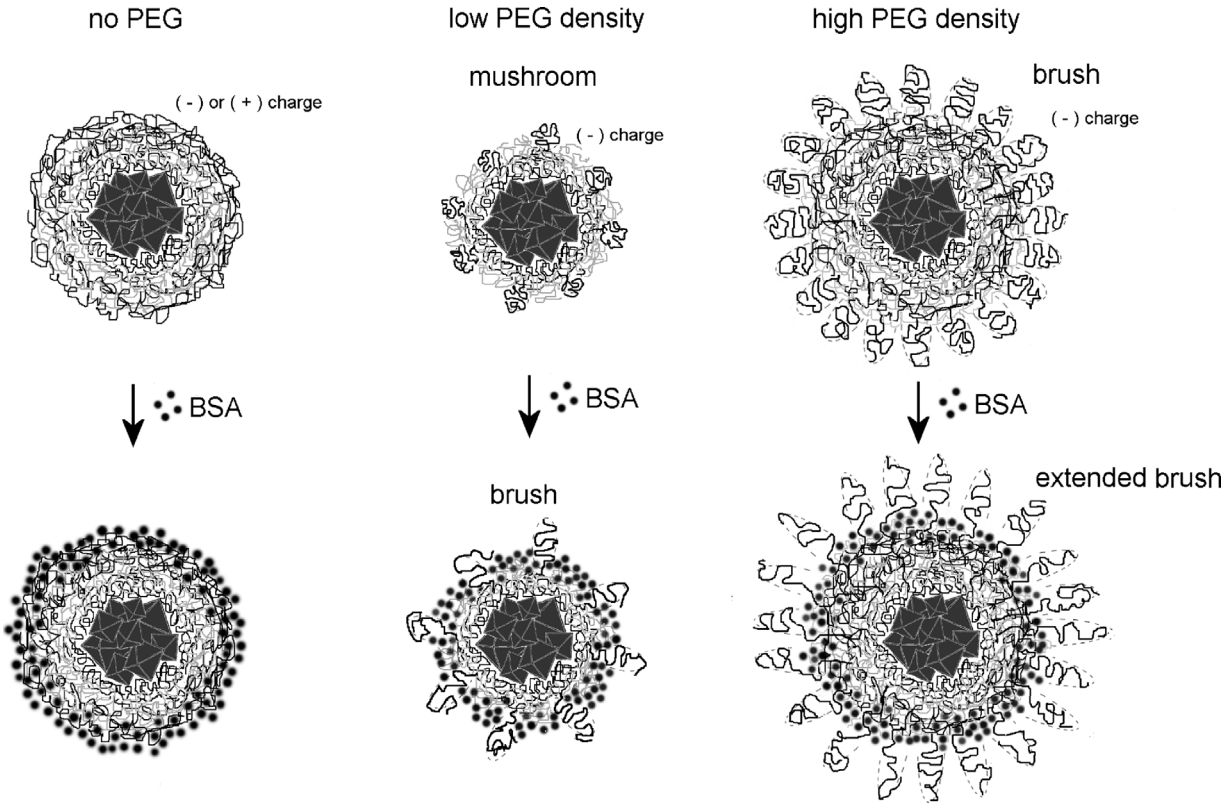

Fig. 8. Possible mechanism of synergetic effect of CHx-PEG and BSA on the stability of LbL nanocapsules.

either slowly diffuses inside polyelectrolyte shell layers [45], peptizing them, or changes the conformation in which it adsorbed on the surface of the LbL coating to more hydrophilic [68]. Both above mentioned mechanisms are possible for CH18-based nanocapsules. In the nanocapsules on the basis of copolymer, some PEG chains are initially hidden beneath or within the thick BSA layer. They slowly rearrange in a more stretched conformation and additional tails appear on the shell surface above a BSA corona.

4. Conclusions

The ultrasound-assisted preparation of MNP/CH colloids is one-step and simple in comparison with LbL nanocapsules. However, a single CH layer provides a temporary stabilization of magnetite nanoparticles in aqueous solutions with the zero ionic strength. The aggregative stability of the MNP/CH colloids in water is low and persists for a relatively long time only for low molecular weight chitosans. The MNP/CH nanoparticles aggregate in FBS and precipitate rapidly in a NaCl solution.

To the contrary, aggregative stability of LbL nanocapsules in biorelevant media can be controlled by varying shell structure and composition. The particular characteristics of MNP/$(CH/PSS)_n$ nanocapsules with a preset shell architecture exceed those for CH-stabilized MNP. The MNP/$(CH/PSS)_n$ nanocapsules on the basis of low molecular weight chitosans or their copolymers with an integer number of bilayers that brings a high negative charge to their surface is the best choice if high colloidal stability is necessary.

Using copolymers of chitosan with PEG in LbL shells has both advantages and certain disadvantages. The CHx-PEG facilitates the preparation of PSS-terminated MNP/$(CH/PSS)_n$ nanocapsules avoiding their aggregation in the process of LbL assembly. The effect is more distinguishable for copolymers of high and medium molecular weight chitosan as compared with parent CHx. As a disadvantage, the colloids of copolymer-terminated nanocapsules deteriorate rapidly.

The synergetic effect of copolymer and albumin on stability of PSS-terminated nanocapsules the shell of which contains one-two CHx-PEG/PSS bilayer greatly simplifies preparation of functional nanoparticles. The stable colloids are obtained after fewer adsorption cycles. Furthermore, based on the proposed mechanism of LbL shell stabilization by a copolymer/BSA system, an interesting assumption can be made. It is not necessary to use copolymer with a high degree of amine group substitution by PEG. If a sufficient number of bilayers are formed and followed by adsorption of a BSA corona, stable LbL nanocapsules can be obtained on the basis of polyelectrolytes that are slightly modified with PEG.

The obtained results are in good consistency with observations on enhanced properties of other BSA-PEG systems. BSA covalently modified at multiple sites by PEG demonstrates increased osmotic activity and better retention within the vasculature than unmodified albumin [70]. Hybrid multi-arm PEG–BSA nanogels exhibit better protein and detergent adsorption resistant properties than covalently coupled BSA surfaces and monolayers of multi-arm PEG [71]. In turn, we have demonstrated that by simultaneously using albumin and copolymers of chitosan and PEG in a LbL shell and varying its architecture the diameter of the obtained nanocapsules and their aggregative-sedimentative stability in biorelevant media can be controlled.

We presume that application of copolymers of other hydrophilic pharmaceutically acceptable polymers such as dextran, polyvinyl alcohol, polyvinylpyrrolidone, etc. can significantly improve stability of LbL-based nanoparticulated forms of biologically active substances and contrast agents. LbL shells based on copolymers are prospective for controlling the interaction of nanocapsules with the body's immune system and distribution in tissues. provide surfaces with low adsorption of biological macromolecules and can be further modified for specific cell targeting.

Acknowledgements

This work was supported by grant 2.09 from the State Program of Scientific Research (SPSR) "Chemical technologies and materials" for 2016–2020, subprogram "Biologically active substances", the Republic of Belarus.

Appendix A. Supplementary data

Supplementary data associated with this article can be found, in the online version, at https://doi.org/10.1016/j.colsurfa.2017.12.008.

References

[1] M.L. Etheridge, S.A. Campbell, A.G. Erdman, C.L. Haynes, S.M. Wolf, J. McCullough, The big picture on nanomedicine: the state of investigational and approved nanomedicine products, Nanomedicine 9 (1) (2013) 1–14, http://dx.doi.org/10.1016/j.nano.2012.05.013.
[2] P.P. Karmali, D. Simberg, Interactions of nanoparticles with plasma proteins: implication on clearance and toxicity of drug delivery systems, Expert Opin. Drug Deliv. 8 (3) (2011) 343–357, http://dx.doi.org/10.1517/17425247.2011.554818.
[3] R. Hao, R. Xing, Z. Xu, Y. Hou, S. Gao, S. Sun, Synthesis, functionalization, and biomedical applications of multifunctional magnetic nanoparticles, Adv. Mater. 22 (25) (2010) 2729–2742, http://dx.doi.org/10.1002/adma.201000260.
[4] L. Li, W. Jiang, K. Luo, H. Song, F. Lan, Y. Wu, Z. Gu, Superparamagnetic iron oxide nanoparticles as MRI contrast agents for non-invasive stem cell labeling and tracking, Theranostics 3 (8) (2013) 595–615, http://dx.doi.org/10.7150/thno.5366.
[5] N. Hildebrandt, C.M. Spillmann, W.R. Algar, T. Pons, M.H. Stewart, E. Oh, K. Susumu, S.A. Díaz, J.B. Delehanty, I.L. Medintz, Energy transfer with semiconductor quantum dot bioconjugates: a versatile platform for biosensing, energy harvesting, and other developing applications, Chem. Rev. 117 (2) (2017) 536–711, http://dx.doi.org/10.1021/acs.chemrev.6b00030.
[6] J.I. Hare, T. Lammers, M.B. Ashford, S. Puri, G. Storm, S.T. Barry, Challenges and strategies in anti-cancer nanomedicine development: an industry perspective, Adv. Drug Deliv. Rev. 108 (1) (2017) 25–38, http://dx.doi.org/10.1016/j.addr.2016.04.025.
[7] V.F. Razumov, Fundamental problems of the chemistry of supramolecular and nanosized structures, Russ. Chem. Bull. Int. Ed. 61 (7) (2012) 1276–1284, http://dx.doi.org/10.1007/s11172-012-0175-6.
[8] M. Komiyama, K. Yoshimoto, M. Sisido, K. Ariga, Chemistry can make strict and fuzzy controls for bio-systems: DNA nanoarchitectonics and cell-macromolecular nanoarchitectonics, Bull. Chem. Soc. Jpn. 90 (9) (2017) 967–1004, http://dx.doi.org/10.1246/bcsj.20170156.
[9] K. Matsuura, Construction of functional biomaterials by biomolecular self-assembly, Bull. Chem. Soc. Jpn. 90 (8) (2017) 873–884, http://dx.doi.org/10.1246/bcsj.20170133.
[10] T.L. Moore, L. Rodriguez-Lorenzo, V. Hirsch, S. Balog, D. Urban, C. Jud, B. Rothen-Rutishauser, M. Lattuada, A. Petri-Fink, Nanoparticle colloidal stability in cell culture media and impact on cellular interactions, Chem. Soc. Rev. 44 (17) (2015) 6287–6305, http://dx.doi.org/10.1039/c4cs00487f.
[11] F. Babick, Suspensions of Colloidal Particles and Aggregates, Springer, 2016, http://dx.doi.org/10.1007/978-3-319-30663-6 ISBN 978-3-319-30663-6.
[12] A.R. Studart, E. Amstad, L.J. Gauckler, Colloidal stabilization of nanoparticles in concentrated suspensions, Langmuir 23 (3) (2007) 1081–1090, http://dx.doi.org/10.1021/la062042s.
[13] T.G. Shutava, G. Parekh, Y.M. Lvov, Core–Shell Drug and Contrast Agent Nanocolloids Through Layer-by-Layer Assembly, in: H.S. Nalwa (Ed.), Encyclopedia of Nanoscience and Nanotechnology, 30-Vol. Set, vol. 26-30, Ch. 4 (2017), ISBN: 1-58883-001-2 (vol.1-10)/1-58883-159-0 (vol.11-25)/1-58883-212-0 (vol.26-30). Corrected proof.
[14] S. Hirsjärvi, Y. Qiao, A. Royere, J. Bibette, J.-P. Benoit, Layer-by-layer surface modification of lipid nanocapsules, Eur. J. Pharm. Biopharm. 76 (2) (2010) 200–207, http://dx.doi.org/10.1016/j.ejpb.2010.07.010.
[15] G. Schneider, G. Decher, Functional core/shell nanoparticles via layer-by-layer assembly. Investigation of the experimental parameters for controlling particle aggregation and for enhancing dispersion stability, Langmuir 24 (5) (2008) 1778–1789, http://dx.doi.org/10.1021/la7021837.
[16] G. Bantchev, Z. Lu, Y. Lvov, Layer-by-layer nanoshell assembly on colloids through simplified washless process, J. Nanosci. Nanotechnol. 9 (1) (2009) 396–403, http://dx.doi.org/10.1166/jnn.2009.J055.
[17] T.G. Shutava, P.P. Pattekari, K.A. Arapov, V.P. Torchilin, Y.M. Lvov, Architectural layer-by-layer assembly of drug nanocapsules with PEGylated polyelectrolytes, Soft Matter 8 (36) (2012) 9418–9427, http://dx.doi.org/10.1039/C2SM25683E.
[18] A.C. Santos, P. Pattekari, S. Jesus, F. Veiga, Y. Lvov, A.J. Ribeiro, Sonication-assisted layer-by-layer assembly for low solubility drug nanoformulation, ACS Appl. Mater. Interfaces 7 (15) (2015) 11972–11983, http://dx.doi.org/10.1021/acsami.5b02002.
[19] S. Abbas, E. Karangwa, M. Bashari, K. Hayat, X. Hong, H.R. Sharif, X. Zhang, Fabrication of polymeric nanocapsules from curcumin-loaded nanoemulsion templates by self-assembly, Ultrason. Sonochem. 23 (2015) 81–92, http://dx.doi.org/10.1016/j.ultsonch.2014.10.006.
[20] A.M. Díez-Pascual, J.E. Wong, Effect of layer-by-layer confinement of polypeptides and polysaccharides onto thermoresponsive microgels: a comparative study, J. Colloid Interface Sci. 347 (1) (2010) 79–89, http://dx.doi.org/10.1016/j.jcis.2010.03.042.

[21] R. Georgieva, R. Dimova, G. Sukhorukov, G. Ibarz, H. Möhwald, Influence of different salts on micro-sized polyelectrolyte hollow capsules, J. Mater. Chem. 15 (40) (2005) 4301–4310, http://dx.doi.org/10.1039/B507848B.

[22] C. Gao, S. Leporatti, E. Donath, H. Möhwald, Surface texture of poly(styrenesulfonate sodium salt) and poly(diallyldimethylammonium chloride) micron-sized multilayer capsules: a scanning force and confocal microscopy study, J. Phys. Chem. B 104 (30) (2000) 7144–7149, http://dx.doi.org/10.1021/jp000615i.

[23] R. Zhang, K. Köhler, O. Kreft, A. Skirtach, H. Möhwald, G. Sukhorukov, Salt-induced fusion of microcapsules of polyelectrolytes, Soft Matter 6 (19) (2010) 4742–4747, http://dx.doi.org/10.1039/C0SM00218F.

[24] J. Shao, M. Xuan, L. Dai, T. Si, J. Li, Q. He, Near-infrared-activated nanocalorifiers in microcapsules: vapor bubble generation for In vivo enhanced cancer therapy, Angew. Chem. Int. Ed. 54 (43) (2015) 12782–12787, http://dx.doi.org/10.1002/anie.201506115.

[25] J. Shao, M. Xuan, T. Si, L. Dai, Q. He, Biointerfacing polymeric microcapsules for *In vivo* near-infrared light-triggered drug release, Nanoscale 7 (45) (2015) 19092–19098, http://dx.doi.org/10.1039/C5NR06350G.

[26] M. Xuan, J. Zhao, J. Shao, C. Du, W. Cui, L. Duan, W. Qi, J. Li, Recent progresses in layer-by-layer assembled biogenic capsules and their applications, J. Colloid Interface Sci. 487 (2017) 107–117, http://dx.doi.org/10.1016/j.jcis.2016.10.018.

[27] W. Knoll, R.C. Advincula (Eds.), Functional Polymer Films, Wiley-VCH Verlag, 2013ISBN: 978-3-527-32190-2.

[28] L. De Matteis, M. Alleva, I. Serrano-Sevilla, S. Garcia-Embid, G. Stepien, M. Moros, J.M. de la Fuente, Controlling properties and cytotoxicity of chitosan nanocapsules by chemical grafting, Mar. Drugs 14 (10) (2016), http://dx.doi.org/10.3390/md14100175 175(15).

[29] T.G. Shutava, A.A. Mastich, K.S. Livanovich, Multilayer films of the poly(ethylene glycol)-modified polysaccharides, Proc. BSU 9 (1) (2014) 101–109.

[30] Y. Jian, X. Xu, Y. Li, Z. Gu, Effect of serum on PEGylated quantum dots: cellular uptake and intracellular distribution, Prog. Nat. Sci. 23 (6) (2013) 566–572, http://dx.doi.org/10.1016/j.pnsc.2013.11.012.

[31] D. Usov, G.B. Sukhorukov, Dextran coatings for aggregation control of layer-by-layer assembled polyelectrolyte microcapsules, Langmuir 26 (15) (2010) 12575–12584, http://dx.doi.org/10.1021/la1018949.

[32] G. Parekh, P. Pattekari, C. Joshi, T. Shutava, M. DeCoster, T. Levchenko, V. Torchilin, Y. Lvov, Layer-by-layer nanoencapsulation of camptothecin with improved activity, Int. J. Pharm. 465 (1–2) (2014) 218–227, http://dx.doi.org/10.1016/j.ijpharm.2014.01.041.

[33] G. Romero, R.A. Murray, Y. Qiu, D. Sanz, S.E. Moya, Layer-by-layer surface engineering of poly(lactide-co-glycolide) nanoparticles: a versatile tool for nanoparticles engineering for targeted drug delivery, Sci. China Chem. Pharm. 56 (8) (2013) 1029–1039, http://dx.doi.org/10.1007/s11426-013-4891-z.

[34] S. Mansouri, Investigation of layer-by-layer assembly of polyelectrolytes on fully functional human red blood cells in suspension for attenuated immune response, Biomacromolecules 12 (3) (2011) 585–592, http://dx.doi.org/10.1021/bm101200c.

[35] U. Wattendorf, O. Kreft, M. Textor, Stealth function for hollow polyelectrolyte microcapsules through a poly(ethylene glycol) grafted polyelectrolyte adlayer, Biomacromolecules 9 (1) (2008) 100–108, http://dx.doi.org/10.1021/bm700857s.

[36] H. Ai, J.J. Pink, X. Shuai, D.A. Boothman, J. Gao, Interactions between self-assembled polyelectrolyte shells and tumor cells, J. Biomed. Mater. Res. 73A (3) (2005) 303–312, http://dx.doi.org/10.1002/jbm.a.30289.

[37] N. Nuraje, R. Asmatulu, R.E. Cohen, M.F. Rubner, Durable antifog films from layer-by-layer molecularly blended hydrophilic polysaccharides, Langmuir 27 (1) (2011) 782–791, http://dx.doi.org/10.1021/la103754a.

[38] L. Xie, W. Tong, D. Yu, J. Xu, J. Li, C. Gao, Bovine serum albumin nanoparticles with multilayers and aptamers for pH-responsive and targeted anti-cancer drug delivery, J. Mater. Chem. 22 (13) (2012) 6053–6060, http://dx.doi.org/10.1039/C2JM16831F.

[39] C. Cortez, J.F. Quinn, X. Hao, C.S. gudipati, M.H. Stenzel, T.P. Davis, F. Caruso, Multilayer buildup and biofouling characteristics of PSS-b-PEG containing films, Langmuir 26 (12) (2010) 9720–9727, http://dx.doi.org/10.1021/la100430g.

[40] R.J. Alekseev, A.L. Rebane (Eds.), Serum Albumin: Structure, Functions, and Health Impact, Nova Science Publ., 2005ISBN: 978-1-62100-298-7.

[41] D. Bazile, C. Ropert, P. Huve, T. Verrecchia, M. Mariard, A. Frydman, M. Veillard, G. Spenlehauer, Body distribution of fully biodegradable [14C]-poly (lactic acid) nanoparticles coated with albumin after parenteral administration to rats, Biomaterials 13 (15) (1992) 1093–1102, http://dx.doi.org/10.1016/0142-9612(92)90142-B.

[42] S. Manoochehri, B. Darvishi, G. Kamalinia, M. Amini, M. Fallah, S.N. Ostad, F. Atyabi, R. Dinarvand, Surface modification of PLGA nanoparticles via human serum albumin conjugation for controlled delivery of docetaxel, DARU J. Pharm. Sci. 21 (1) (2013) 58–67, http://dx.doi.org/10.1186/2008-2231-21-58.

[43] A.B. Kayitmazer, S.P. Strand, C. Tribet, W. Jaeger, P.L. Dubin, Effect of polyelectrolyte structure on protein-polyelectrolyte coacervates: coacervates of bovine serum albumin with poly (diallyldimethylammonium chloride) versus chitosan, Biomacromolecules 8 (11) (2007) 3568–3577, http://dx.doi.org/10.1021/bm700645t.

[44] Y. Budama Battal, M. Topuzogullari, Z. Mustafaeva, The fluorescence study of interaction between bovine serum albumin and polyacrylic acid, J. Fluoresc. (2009) 1–11, http://dx.doi.org/10.1007/s10895-009-0484-9.

[45] G. Ladam, C. Gergely, B. Senger, G. Decher, J.-C. Voegel, P. Schaaf, F.J.G. Cuisinier, Protein interactions with polyelectrolyte multilayers: interactions between human serum albumin and polystyrene sulfonate/polyallylamine multilayers, Biomacromolecules 1 (4) (2000) 674–687, http://dx.doi.org/10.1021/bm005572q.

[46] M. Kumorek, D. Kubies, T. Riedel, Protein interactions with quaternized chitosan/heparin multilayers, Physiol. Res. 65 (2) (2016) S253–S261.

[47] V.V. Pankov, T.G. Shutava, K.S. Livanovich, D.A. Kotsikau, E.G. Petrova, V.O. Natarov, S.V. Trukhanov, $(Mg, Zn)_xFe_{3-x}O_4$ nanoparticles: synthesis, magnetic properties, surface functionalization, Proc. Natl. Acad. Sci. Belarus Chem. Ser. 2 (2017) 15–24.

[48] Yu. V. Bogachev, A.V. Nikitina, A.A. Kostina, V.A. Sabitova, V.V. Pankov, T.G. Shutava, E.G. Petrova, D.A. Kotsikau, V.O. Natarov, K.S. Livanovich, NMR relaxation efficiency of aqueous solutions of composite $Mg_xZnyFe_{3-x-y}O_4$ nanoparticles, Appl. Magn. Reson. 48 (7) (2017) 715–722, http://dx.doi.org/10.1007/s00723-017-0889-6.

[49] A.V. Il'ina, V.P. Varlamov, Hydrolysis of chitosan in lactic acid, Appl. Biochem. Microbiol. 40 (3) (2004) 300–303, http://dx.doi.org/10.1023/B:ABIM.0000025956.98250.30.

[50] R. Czechowska-Biskup, D. Jarosinska, B. Rokita, P. Ulanski, J.M. Rosiak, Determination of degree of deacetylation of chitosan-comparision of methods, Prog. Chem. Appl. Chitin Deriv. 17 (2012) 5–20.

[51] M.V. Volkenstein, Molecular Biophysics, Academic Press, Inc., 1977, pp. 326–334 ISBN: 978-0124125032.

[52] N. Ueyama, M. Nakata, A. Nakamura, A poly(oxyethylene)-supported Cys-Pro-Leu-Cys/Fe(II) complex as a rubredoxin model: protection of the Fe-Cys coordination from hydrolysis in aqueous solution, Polym. J. 17 (5) (1985) 721–727, http://dx.doi.org/10.1295/polymj.17.721.

[53] H. Du, P.-K. Lo, Z. Hu, H. Liang, K.-C. Lau, Y.-N. Wang, W.W.Y. Lam, T.-C. Lau, Lewis-acid – activated oxidation of alcohols by permanganate, Chem. Commun. 47 (25) (2011) 7143–7145, http://dx.doi.org/10.1039/C1CC12024G.

[54] J. Bartos, Colorimetric determination of organic compounds by formation of hydroxamic acids, Talanta 27 (7) (1980) 583–590, http://dx.doi.org/10.1016/0039-9140(80)80183-4.

[55] G. Hermanson, Bioconjugate Techniques, 2nd ed., Elsevier, 2008, pp. 215–222 ISBN: 9780123705013.

[56] T.G. Shutava, V.I. Kulikouskaya, P.H. Hai, T.D. Toai, P.Q. Long, V.E. Agabekov, Structure and properties of κ-carrageenan from red seaweed *Eucheuma gelatina*, Proc. Natl. Acad. Sci. Belarus Chem. Ser. 4 (2011) 62–67.

[57] W.B. Fortune, M.G. Mellon, Determination of iron with o-phenanthroline: a spectrophotometric study, Ind. Eng. Chem. Anal. Ed. 10 (2) (1938) 60–64, http://dx.doi.org/10.1021/ac50118a004.

[58] D. Cocke, Interaction between poly (ethylene glycol) and human serum albumin, Chem. Commun. 23 (1997) 2331–2332, http://dx.doi.org/10.1039/A706040H.

[59] L. Bekale, D. Agudelo, H. Tajmir-Riahi, The role of polymer size and hydrophobic end-group in PEG–protein interaction, Colloids Surf. B 130 (2015) 141–148, http://dx.doi.org/10.1016/j.colsurfb.2015.03.045.

[60] U. Sakulkhu, M. Mahmoudi, L. Maurizi, J. Salaklang, H. Hofmann, Protein corona composition of superparamagnetic iron oxide nanoparticles with various physico-chemical properties and coatings, Sci. Rep. 4 (2014) 5020, http://dx.doi.org/10.1038/srep05020.

[61] S.B. Abbott, W.M. de Vos, L.L.E. Mears, R. Barker, R.M. Richardson, S.W. Prescott, Hydration of odd–even terminated polyelectrolyte multilayers under mechanical confinement, Macromolecules 47 (10) (2014) 3263–3273, http://dx.doi.org/10.1021/ma500557m.

[62] C. Picart, Polyelectrolyte multilayer films: from physico-chemical properties to the control of cellular processes, Curr. Med. Chem. 15 (7) (2008) 685–697, http://dx.doi.org/10.1002/adfm.200701297.

[63] S. Lüsse, K. Arnold, The interaction of poly(ethylene glycol) with water studied by 1H and 2H NMR relaxation time measurements, Macromolecules 29 (12) (1996) 4251–4257, http://dx.doi.org/10.1021/ma9508616.

[64] E.M. Mazzaferroo, E. Rudloff, R. Kirby, The role of albumin replacement in the critically ill veterinary patient, J. Vet. Emerg. Crit. Care 12 (2) (2002) 113–124, http://dx.doi.org/10.1046/j.1435-6935.2002.00025.x.

[65] J.W. Bye, S. Meliga, D. Ferachou, G. Cinque, J.A. Zeitler, R.J. Falconer, Analysis of the hydration water around bovine serum albumin using terahertz coherent synchrotron radiation, J. Phys. Chem. A 118 (1) (2014) 83–88, http://dx.doi.org/10.1021/jp407410g.

[66] O. Sushko, R. Dubrovka, R.S. Donnan, Sub-terahertz spectroscopy reveals that proteins influence the properties of water at greater distances than previously detected, J. Chem. Phys. 142 (5) (2015) 055101, http://dx.doi.org/10.1063/1.4907271.

[67] S. Kiihne, R.G. Bryant, Protein-bound water molecule counting by resolution of ^1H spin-lattice relaxation mechanisms, Biophys. J. 78 (4) (2000) 2163–2169, http://dx.doi.org/10.1016/S0006-3495(00)76763-4.

[68] J.A. Molina-Bolivar, J.L. Ortega-Vinuesa, How proteins stabilize colloidal particles by means of hydration forces, Langmuir 15 (8) (1999) 2644–2653, http://dx.doi.org/10.1021/la981445s.

[69] J.L. Perry, K.G. Reuter, M.P. Kai, K.P. Herlihy, S.W. Jones, J.C. Luft, M. Napier, J.E. Bear, J.M. DeSimone, PEGylated PRINT nanoparticles: the impact of PEG density on protein binding, macrophage association, biodistribution, and pharmacokinetics, Nano Lett. 12 (10) (2012) 5304–5310, http://dx.doi.org/10.1021/nl302638g.

[70] R.A. Assaly, M. Azizi, D.J. Kennedy, C. Amauro, A. Zaher, F.W. Houts, R.H. Habib, J.I. Shapiro, J.D. Dignam, Plasma expansion by polyethylene-glycol-modified albumin, Clin. Sci. 107 (3) (2004) 263–272, http://dx.doi.org/10.1042/CS20040001.

[71] C.D. Donahoe, T.L. Cohen, W. Li, P.K. Nguyen, J.D. Fortner, R.D. Mitra, D.L. Elbert, Ultralow protein adsorbing coatings from clickable PEG nanogel solutions: benefits of attachment under salt-induced phase separation conditions and comparison with PEG/albumin nanogel coatings, Langmuir 29 (12) (2013) 4128–4139, http://dx.doi.org/10.1021/la3051115.